International Journal of Power Electronics and Drive Systems (IJPEDS)
Vol. 7, No. 2, June 2016, pp. 279 – 293
ISSN: 2088-8694

Single-Switch Soft-Switched Boost Power Factor Corrector for Modular Applications

Toms A. Gonzlez[*], Daniel O. Mercuri[*], Hernn E. Tacca[*], and Mximo E. Pupareli[**]
[*]Department of Electronics, Faculty of Engineering, University of Buenos Aires.
[**]HT. S.A., Argentina.

Article Info

Article history:
Received Nov 14, 2015
Revised Feb 13, 2016
Accepted Feb 27, 2016

Keyword:
Power factor corrector
Boost converter
Soft-switching
Passive non-dissipative snubber

ABSTRACT

Modern dc power supplies provide power factor correction but the classical two-stage approach, using hard-switched preregulators, has detrimental effects on efficiency and reliability, particularly for high power applications. With some circuit modifications and the addition of a few magnetic components, diodes and capacitors, we have turned a classical boost power factor corrector into a high efficiency soft-switched version. The proposed converter turns on its single switch with zero current and turns it off with zero voltage. In this paper we explain the proposed changes, we study the waveforms and equations and we verify them with an experimental prototype. We also show how the converter can be used for modular single- and three-phase high power applications.

Corresponding Author:
Toms A. Gonzlez.
Department of Electronics, Faculty of Engineering, UBA
Av. Paseo Coln 850, C1063ACV, Buenos Aires, Argentina.
Tel: +54 (11) 4343-0893 / 4343-0092
tgonzalez@fi.uba.ar

1. INTRODUCTION

Conventional power supplies exhibit low power factor and produce harmonic pollution of the mains. In high power applications, passive filtering becomes nonviable due to the increasing size and weight of the required components, such as low frequency line filters and capacitor banks. Nowadays, power electronic conversion techniques facilitate the use of active power factor correction methods and circuits, known as PWM rectifiers [1].

The boost converter is one of the most used topologies in PWM rectifiers[2, 3, 4]. Single phase dc power supplies are usually composed of the boost front-end or preregulator produces near unity power factor and an intermediate high voltage bus and an isolated dc-dc converter to supply the desired output voltage regulation. At high power, the efficiency of the front end is a key characteristic. Many high efficiency boost converters have been developed in the past using soft-switching techniques [5, 6, 7, 8, 9, 10, 11, 12, 13, 14, 15, 16]; some of them use auxiliary switches[5, 6, 7, 8, 9, 10, 11, 12], making them more complex and less reliable. Passive soft-switching techniques combine higher reliability and simplicity of design [13, 14, 15]. The power supply manufacturer saves not only the cost of auxiliary switches, but also the development of a specific integrated circuit to drive them [17].

Modularization is an attractive technique for power converter manufacturers and users since it provides redundancy, flexibility, reduction of manufacturing cost and time [18];it also applies to power supplies with power factor correction. Paralleling single phase converters in order to get a higher power supply was shown in [19] with boost converters. Several fields exist where this is a useful practice: single phase railway systems [20] or L1/L2 battery chargers for plug-in electric and hybrid vehicles [21]. Another example of modularization are three-phase power supplies manufactured from single phase modules [22, 9, 13].

This paper introduces a boost-derived preregulator with novel passive soft-switching networks and shows its application to modular high power converters. Zero Voltage Switching (ZVS) at turn-off and Zero Current Switching (ZCS) at turn-on provide a reduction in losses compared to a classic boost converter [1].

In Section 2. we present the proposed circuit and we make qualitative and quantitative analyses to derive its principle of operation, waveforms and characterizing equations. Next, we describe the experimental results of a single

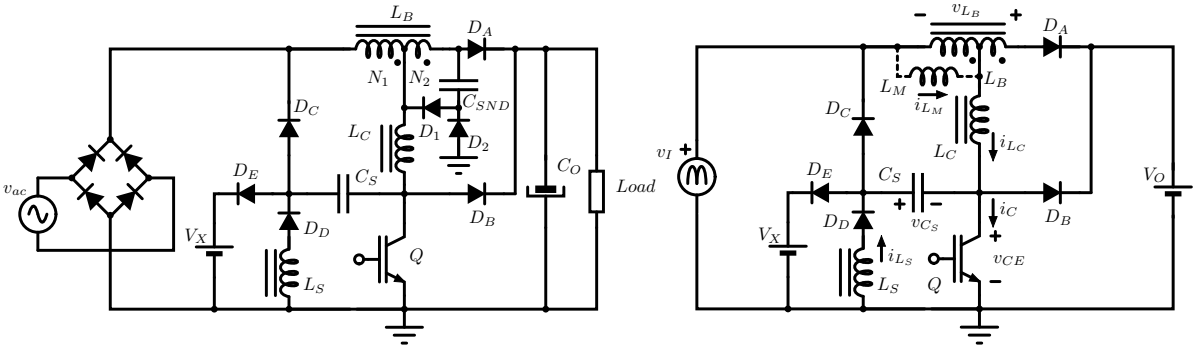

(a) Schematic circuit.

(b) Simplified model with voltage and current reference directions.

Figure 1. Boost power factor corrector basic module.

module in Section 3.. Finally, in Section 4., we explain the considerations that should be accounted for in order to use the converter in a modular approach.

2. BOOST PFC SOFT-SWITCHED MODULE AND ITS PRINCIPLE OF OPERATION.

Figure 1a shows the considered module. The circuit composed of D_1, D_2, and C_{SND} acts as a lossless snubber for diode D_A; it allows the discharge of the stored energy remaining in the secondary leakage inductance of inductor L_B. D_B, D_C, D_D, C_S, L_S and L_C comprises the basic soft-switching networks. A voltage source, V_X, connected through diode D_E enables the transistor to switch softly throughout the entire input voltage cycle. We will discuss the need of this source, its implementation and value in the following sections.

The circuit is based on the tapped boost converter, with a transfer function given by:

$$\frac{V_O}{v_I} = \frac{1 + d(t)\frac{N_2}{N_1}}{1 - d(t)}, \tag{1}$$

which approximates the classical boost transfer function when $N_1 > N_2$ and still produces a step up characteristic. Thus, it is possible to use boost PFC commercial controllers [23] with average current mode control [1] in order to regulate the output voltage and make the input current follow the input voltage waveform.

The simplified circuital model of Figure 1b allows us to perform the following qualitative and quantitative analyses of the switching process.

2.1. Qualitative analysis

If $v_I < V_X$, the circuit is in mode I. When the IGBT turn-off occurs, at $t = t_0$, the circuit transitions from the conduction state shown in Figure 2a to the first state of the turn-off process shown in Figure 2b. The inductance of both L_B and L_C force diode D_C to carry the magnetizing current. Starting from $v_I - v_{C_S}(t_0)$, v_{CE} rises linearly due to the constant current discharging of C_S. In order to ensure zero voltage switching $v_{C_S}(t_0)$ must be equal to v_I.

At $t = t_1$, v_{L_B} reaches $V_O - v_I$ and turns diode D_A on. C_S keeps discharging through L_C and v_{CE} further rises (Figure2c) until $v_{CE} = V_O$ and $v_{C_S} = v_I - V_O$, at $t = t_2$; D_B turns on and L_C discharges the stored energy to the load (Figure2f). When $i_{L_C} = 0$ A at $t = t_3$, the turn-off ends and the state of Figure 2g starts.

After the switch turns on at $t = t_4$, its current starts rising gradually due to L_C; zero current switching occurs. Simultaneously, the LC resonance of C_S and L_S inverts the polarity of v_{C_S} (Figure2h). If $V_O - v_I > v_I$, the diode D_C turns on before the complete discharge of L_S, v_{C_S} clamps at v_I, and the state pictured in Figure 2j starts. The previous condition is equivalent to $v_I < V_O/2$ and it is of paramount importance because it guarantees the starting value of v_{C_S} in the next switching cycle to produce the ZVS turn-off of the converter.

The purpose of the voltage source V_X is to provide ZVS turn-off for $v_I > V_O/2$. The idea is to clamp the voltage of C_S to a value lower than v_I, since diode D_C will not be able to turn on. In order to clarify this, we will explore mode II that occurs for $v_I > V_X$.

At $t = t_0$, the transistor turns off and the converter enters the state shown in Figure 2d. In this mode, the magnetizing current flows through D_E and transfers energy to V_X. As in mode I, v_{CE} and v_{C_S} start rising linearly but $v_{C_S}(t_0)$ should be equal to V_X so as to ensure ZVS turn-off. At $t = t_1$, the state pictured in Figure 2e starts: v_{L_B} turns

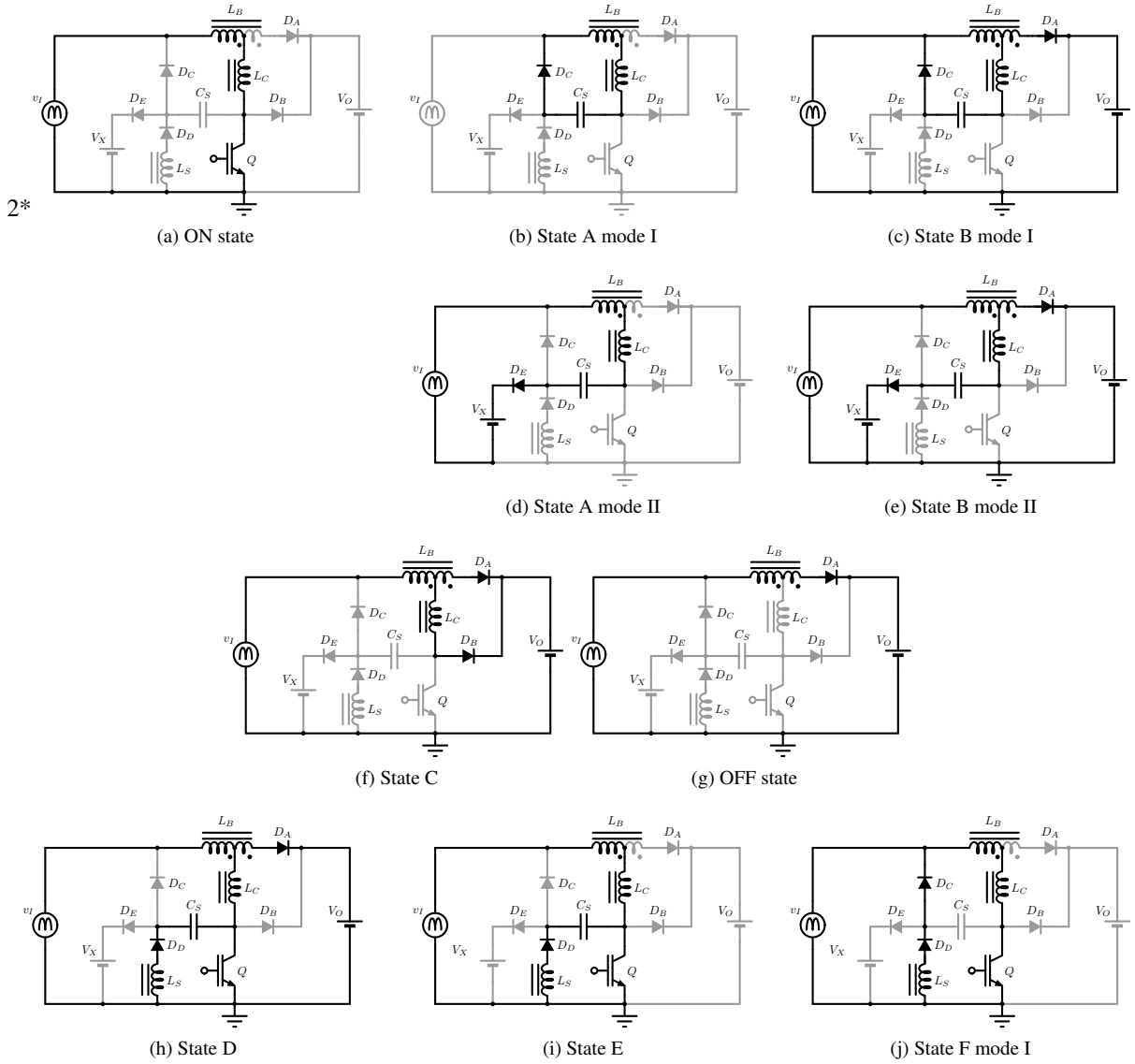

Figure 2. Operating states in mode I ($v_I < V_X$) and mode II ($v_I > V_X$).

D_A on, taking the magnetizing current, and C_S continues its charge through L_C. The final state of turn-off, shown in Figure 2f, starts at t_2 when $v_{CE} = V_O$. D_B turns on and L_C discharges to the output as in mode I.

The ZCS turn-on process is similar as before and presented in Figures 2h and 2i. The difference is that the last state is missing, because the resonant oscillation of v_{C_S} lasts until D_C turns off. v_{C_S} reverts its polarity to V_X, the required value for ZVS turn-off to occur.

In order to guarantee ZVS for all values of input voltage, V_X should take a value that introduces the circuit to mode II if $v_I > V_O/2$:

$$V_X \leq \frac{V_O}{2}. \tag{2}$$

If $V_X = V_O/2$, mode I occurs for $v_I < V_O/2$ and mode II for $v_I > V_O/2$. Selecting a smaller value for V_X produces an additional transfer of energy to this source when $v_I > V_O/2$. As this energy should be dissipated or sent back to the source, it is important to minimize it by adopting $V_X = V_O/2$. This condition will be better explained in the quantitative analysis of the following section.

The tapped boost configuration allows in both modes the discharge of the energy stored in L_C at the end of the switching cycle, thus providing ZCS turn-on.

2.2. Quantitative analysis: equations and waveforms

By considering that the switching frequency is much higher than the line frequency, we employ an approximately constant value of v_I for each switching period. Also, we neglect output voltage ripple:$v_O \simeq V_O \simeq$ constant.

The controller modulates the transistor duty-cycle $d(t)$ to produce $i_{L_M}(t) \simeq I_{I_{max}} |\sin(\omega t)|$. As a result, we regard i_{L_M} as constant during the switching cycle, also neglecting the current ripple. We also neglect transistor and diode voltage drops and parasitic capacitances.

2.2.1. Mode I

- $t_0 < t \leq t_1$ (Figure2b): The solution for v_{C_S} is

$$v_{C_S}(t) = v_{C_S}(t_0) + \frac{1}{C_S}\int_{t_0}^{t} i_{C_S} d\tau = v_{C_S}(t_0) - \frac{i_{L_M}}{C_S}(t - t_0). \tag{3}$$

The transistor voltage rises following

$$v_{CE}(t) = v_I - v_{C_S}(t) = v_I - v_{C_S}(t_0) + \frac{i_{L_M}}{C_S}(t - t_0), \tag{4}$$

where the ZVS condition arises

$$v_{CE}(t_0) = 0 \iff v_{C_S}(t_0) = v_I, \tag{5}$$

and it follows that

$$v_{CE}(t) = \frac{i_{L_M}}{C_S}(t - t_0). \tag{6}$$

During this time interval $i_C(t) = 0$ and $i_{L_C} = i_{L_M}$, and because we consider i_{L_M} almost constant consequently $v_{LC} = 0$. v_{L_B} rises following the changes in v_{CS} until diode D_A turns on, reaching

$$v_{L_B}(t_1) = V_O - v_I = \frac{N_1 + N_2}{N_1} v_{C_S}(t_1). \tag{7}$$

Using this result and Equation (4) gives

$$v_{C_S}(t_1) = (V_O - v_I)\frac{N_1}{N_1 + N_2} \tag{8}$$

and

$$v_{C_E}(t_1) = v_I - \frac{N_1}{N_1 + N_2}(V_O - v_I), \tag{9}$$

which we can solve for t_1

$$\frac{i_{L_M}}{C_S}(t_1 - t_0) = v_I - \frac{N_1}{N_1 + N_2}(V_O - v_I). \tag{10}$$

- $t_1 < t \leq t_2$ (Figure2c): When diode D_A turns on, the boost inductor imposes a voltage to the series connection of L_C and C_S. C_S charges resonantly according to

$$\frac{d^2 v_{C_S}}{dt^2} + \frac{1}{L_C C_S} v_{C_S} = \frac{(v_I - V_O)}{L_C C_S}\frac{N_1}{N_1 + N_2} \tag{11}$$

with initial conditions

$$v_{C_S}(t_1) = (v_I - V_O)\frac{N_1}{N_1 + N_2}, \tag{12}$$

$$\frac{dv_{C_S}}{dt}(t_1) = -\frac{i_{L_M}}{C_S}. \tag{13}$$

We solve Equation (11) in order to find

$$v_{C_S}(t) = \frac{(v_I - V_O)\, N_1}{N_1 + N_2} - i_{L_M}\sqrt{\frac{L_C}{C_S}}\sin\left(\frac{t - t_1}{\sqrt{L_C C_S}}\right) \tag{14}$$

and

$$v_{C_E}(t) = v_I - (v_I - V_O)\frac{N_1}{N_1+N_2} + i_{L_M}\sqrt{\frac{L_C}{C_S}}\sin\left(\frac{t-t_1}{\sqrt{L_C C_S}}\right). \quad (15)$$

The state evolves as calculated until D_B turns on at time t_2, when

$$v_{CE}(t_2) = V_O, \quad (16)$$

and

$$v_{C_S}(t_2) = v_I - V_O. \quad (17)$$

We can solve Equation (16) for t_2

$$i_{L_M}\sqrt{\frac{L_C}{C_S}}\sin\left(\frac{t_2-t_1}{\sqrt{L_C C_S}}\right) = \frac{(V_O - v_I)N_2}{N_1+N_2}. \quad (18)$$

During this state $i_C = 0$ and i_{L_C} oscillates according to

$$i_{L_C}(t) = -C_S\frac{dv_{C_S}}{dt} = i_{L_M}\cos\left(\frac{t-t_1}{\sqrt{L_C C_S}}\right). \quad (19)$$

- $t_2 < t \leq t_3$ (Figure2f): Through the clamping action of D_B, the energy stored in L_C transfers to the output at constant voltage

$$i_{L_C}(t) = i_{L_C}(t_2) + \frac{1}{L_C}\int_{t_2}^{t}(v_I - V_O)\frac{N_2}{N_1+N_2}d\tau = i_{L_M}\cos\left(\frac{t_2-t_1}{\sqrt{L_C C_S}}\right) - \frac{(V_O-v_I)N_2}{N_1+N_2}\frac{(t-t_2)}{L_C} \quad (20)$$

Meanwhile, $i_C(t) = 0$, $v_{CE}(t) = V_O$, and $v_{C_S}(t) = v_I - V_O$. This state ends at t_3, when D_B turns off; $i_{L_C}(t_3) = 0$. We find t_3 using

$$i_{L_M}\cos\left(\frac{t_2-t_1}{\sqrt{L_C C_S}}\right) - \frac{(V_O-v_I)N_2}{N_1+N_2}\frac{(t_3-t_2)}{L_C} = 0. \quad (21)$$

- $t_3 < t \leq t_4$ (Figure2g). This interval corresponds to the conventional off state of a tapped boost.
- $t_4 < t \leq t_5$ (Figure2h): Transistor Q turns on and its current has two components

$$i_C(t) = i_{L_S}(t) + i_{L_C}(t). \quad (22)$$

We find the first component solving the differential equation

$$\frac{d^2 v_{C_S}}{dt^2} + \frac{1}{L_S C_S}v_{C_S} = 0, \quad (23)$$

$$v_{C_S}(t_4) = v_I - V_O, \quad (24)$$

$$\frac{dv_{C_S}}{dt}(t_4) = 0, \quad (25)$$

which results in

$$v_{C_S}(t) = (v_I - V_O)\cos\left(\frac{t-t_4}{\sqrt{L_S C_S}}\right), \quad (26)$$

and lets us compute

$$i_{L_S}(t) = (v_I - V_O)\sqrt{\frac{C_S}{L_S}}\sin\left(\frac{t-t_4}{\sqrt{L_S C_S}}\right). \quad (27)$$

Simultaneously, L_C starts taking the boost inductor current at constant voltage:

$$i_{L_C}(t) = i_{L_C}(t_4) + \frac{1}{L_C}\int_{t_4}^{t}\left[v_I - \frac{(v_I - V_O)N_1}{N_1+N_2}\right]d\tau = \frac{1}{L_C}\left[v_I - (v_I - V_O)\frac{N_1}{N_1+N_2}\right](t-t_4). \quad (28)$$

This state ends when L_C takes the output current, the whole magnetizing current of the tapped boost inductor, and D_A turns off

$$i_{L_C}(t_5) = i_{L_M} = \frac{1}{L_C}\left[v_I - \frac{(v_I - V_O)\,N_1}{N_1 + N_2}\right](t_5 - t_4). \tag{29}$$

In practice, we have built L_C as a swinging inductor in order to provide a greater inductance for low currents, at the beginning of the turn-on process. At higher currents, the ungapped part of the core saturates, and the inductance reduces. This structure lets us use a smaller core than a non-saturable inductor would require. It can also prevent the destruction of the inductor due to excessive heat dissipation if a fully saturable core were to be used: the non-saturable mass of the core acts as a heat sink if only the partial gap material is saturable. As a result, the current does not rise linearly as stated in Equation (28).

- $t_5 < t \leq t_6$ (Figure2i): The state evolves with current i_{L_S} oscillating according to Equation (27) until diode D_C turns on, when $v_{C_S} = v_I$. To find t_6 we solve

$$v_I = (v_I - V_O)\cos\left(\frac{t_6 - t_4}{\sqrt{L_S C_S}}\right), \tag{30}$$

which has a solution only if $V_O - v_I > v_I$, and leads to the condition

$$v_I < V_O/2. \tag{31}$$

If V_X and D_E were not present, ZVS turn-off would not be possible for $v_I > V_O/2$: the voltage of C_S would not be clamped to v_I at the end of this state, but to $V_O - v_I > v_I$ and the additional voltage would produce a hard turn-off in the following switching cycle. If we somehow fix $V_X = V_O/2$, D_E would turn on for values of v_I larger than $V_O/2$, instead of D_C, and v_{C_S} would be clamped to $V_O/2$. This situation corresponds to mode II.

- $t_6 < t \leq t_7$ (Figure2j): The remaining energy stored in L_S discharges at constant voltage v_I

$$i_{L_S}(t) = i_{L_S}(t_6) - \frac{1}{L_S}\int_{t_6}^{t} v_I d\tau = (V_O - v_I)\sqrt{\frac{C_S}{L_s}}\sin\left(\frac{t_6 - t_4}{\sqrt{L_S C_S}}\right) - \frac{v_I}{L_S}(t - t_6). \tag{32}$$

It ends when diodes D_C and D_D turn-off, at t_7, found from $i_{L_S}(t_7) = 0$

$$(V_O - v_I)\sqrt{\frac{C_S}{L_s}}\sin\left(\frac{t_6 - t_4}{\sqrt{L_S C_S}}\right) - \frac{v_I}{L_S}(t_7 - t_6) = 0. \tag{33}$$

- $t_7 < t \leq T_S + t_0$ (Figure2a) ON-State.

The previously derived waveforms of v_{CE}, i_C, v_{C_S}, i_{L_C}, and i_{L_S} are depicted in Figure 3.

2.2.2. Mode II

As previously derived, we choose $V_X = V_O/2$. This will be considered for the following theoretical analysis and waveform derivations.

- $t_0 < t \leq t_1$ (Figure2d): The solution for v_{C_S} is

$$v_{C_S}(t) = v_{C_S}(t_0) + \frac{1}{C_S}\int_{t_0}^{t} i_{C_S} d\tau = v_{C_S}(t_0) - \frac{i_{L_M}}{C_S}(t - t_0). \tag{34}$$

The transistor voltage rises following

$$v_{CE}(t) = \frac{V_O}{2} - v_{C_S}(t) = \frac{V_O}{2} - v_{C_S}(t_0) + \frac{i_{L_M}}{C_S}(t - t_0), \tag{35}$$

where the ZVS condition arises

$$v_{CE}(t_0) = 0 \iff v_{C_S}(t_0) = \frac{V_O}{2}, \tag{36}$$

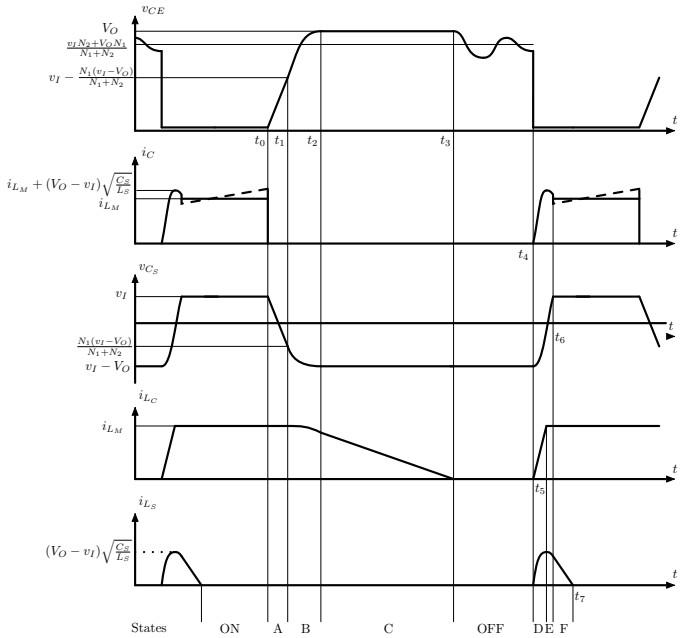

Figure 3. Main voltage and current waveforms for a mode I switching cycle. A dashed line shows a better approximation to the real waveforms, including the current ripple of i_C.

and it follows that

$$v_{CE}(t) = \frac{i_{L_M}}{C_S}(t - t_0). \tag{37}$$

During this time interval $i_C(t) = 0$ and $i_{L_C} = i_{L_M}$, and because we consider i_{L_M} almost constant consequently $v_{LC} = 0$. v_{L_B} rises following the changes in v_{CS} until diode D_A turns on, reaching

$$v_{L_B}(t_1) = V_O - v_I = -\frac{N_1 + N_2}{N_1}\left(\frac{V_O}{2} - v_I - v_{C_S}(t_1)\right). \tag{38}$$

Using this result and Equation (35) gives

$$v_{C_S}(t_1) = \frac{V_O}{2} - v_I - (V_O - v_I)\frac{N_1}{N_1 + N_2}, \tag{39}$$

and

$$v_{C_E}(t_1) = v_I + \frac{N_1}{N_1 + N_2}(V_O - v_I), \tag{40}$$

which we can solve for t_1

$$\frac{i_{L_M}}{C_S}(t_1 - t_0) = v_I + \frac{N_1}{N_1 + N_2}(V_O - v_I). \tag{41}$$

- $t_1 < t \leq t_2$ (Figure2e): When diode D_A turns on, the boost inductor imposes a voltage to the series connection of L_C and C_S. C_S charges resonantly according to

$$\frac{d^2 v_{C_S}}{dt^2} + \frac{1}{L_C C_S} v_{C_S} = \frac{1}{L_C C_S}\left[\frac{V_O}{2} - v_I - (V_O - v_I)\frac{N_1}{N_1 + N_2}\right] \tag{42}$$

with initial conditions

$$v_{C_S}(t_1) = \frac{V_O}{2} - v_I - (V_O - v_I)\frac{N_1}{N_1 + N_2}, \tag{43}$$

$$\frac{dv_{C_S}}{dt}(t_1) = -\frac{i_{L_M}}{C_S}. \tag{44}$$

We can solve Equation (42) in order to find

$$v_{C_S}(t) = \frac{V_O}{2} - v_I - (V_O - v_I)\frac{N_1}{N_1+N_2} - i_{L_M}\sqrt{\frac{L_C}{C_S}}\sin\left(\frac{t-t_1}{\sqrt{L_C C_S}}\right), \tag{45}$$

and

$$v_{C_E}(t) = v_I + (V_O - v_I)\frac{N_1}{N_1+N_2} + i_{L_M}\sqrt{\frac{L_C}{C_S}}\sin\left(\frac{t-t_1}{\sqrt{L_C C_S}}\right). \tag{46}$$

The state evolves as calculated until D_B turns on at time t_2, when

$$v_{CE}(t_2) = V_O, \tag{47}$$

and

$$v_{C_S}(t_2) = \frac{V_O}{2} - V_O = -\frac{V_O}{2}. \tag{48}$$

We can solve Equation (47) for t_2

$$V_O = v_I + (V_O - v_I)\frac{N_1}{N_1+N_2} + i_{L_M}\sqrt{\frac{L_C}{C_S}}\sin\left(\frac{t_2-t_1}{\sqrt{L_C C_S}}\right). \tag{49}$$

During this state $i_C = 0$ and i_{L_C} oscillates according to

$$i_{L_C}(t) = -C_S\frac{dv_{C_S}}{dt} = i_{L_M}\cos\left(\frac{t-t_1}{\sqrt{L_C C_S}}\right). \tag{50}$$

- $t_2 < t \leq t_3$ (Figure2f): Through the clamping action of D_B, the energy stored in L_C transfers to the output at constant voltage

$$i_{L_C}(t) = i_{L_C}(t_2) + \frac{1}{L_C}\int_{t_2}^{t}(v_I - V_O)\frac{N_2}{N_1+N_2}d\tau = i_{L_M}\cos\left(\frac{t_2-t_1}{\sqrt{L_C C_S}}\right) - \frac{(V_O - v_I)N_2}{N_1+N_2}\frac{(t-t_2)}{L_C}. \tag{51}$$

Meanwhile, $i_C(t) = 0$, $v_{CE}(t) = V_O$, and $v_{C_S}(t) = -V_O/2$. This state ends at t_3, when D_B turns off; $i_{L_C}(t_3) = 0$. We find t_3 using

$$i_{L_M}\cos\left(\frac{t_2-t_1}{\sqrt{L_C C_S}}\right) - (V_O - v_I)\frac{N_2}{N_1+N_2}\frac{(t_3-t_2)}{L_C} = 0. \tag{52}$$

- $t_3 < t \leq t_4$ (Figure2g) This interval corresponds to the conventional off state of a tapped boost.
- $t_4 < t \leq t_5$ (Figure2h): Transistor Q turns on and its current has two components

$$i_C(t) = i_{L_S}(t) + i_{L_C}(t). \tag{53}$$

We find the first component solving the differential equation

$$\frac{d^2 v_{C_S}}{dt^2} + \frac{1}{L_S C_S}v_{C_S} = 0, \tag{54}$$

$$v_{C_S}(t_4) = -\frac{V_O}{2}, \tag{55}$$

$$\frac{dv_{C_S}}{dt}(t_4) = 0, \tag{56}$$

which results in

$$v_{C_S}(t) = -\frac{V_O}{2}\cos\left(\frac{t-t_4}{\sqrt{L_S C_S}}\right), \tag{57}$$

and lets us compute

$$i_{L_S}(t) = \frac{V_O}{2}\sqrt{\frac{C_S}{L_S}}\sin\left(\frac{t-t_4}{\sqrt{L_S C_S}}\right). \tag{58}$$

Table 1. Specifications and components of the experimental module.

Specification	Value	Device	Value
P_O	3 kW	Q	IRGP50B60PD1 (600 V/33 A)
v_{ac}	220 V/ 50 Hz	D_A	HFA16TB120 (1200 V/16 A)
V_O	500 V	$D_{B,C,D,1,2,3,5}$	MUR860 (600 V/8 A)
f_S	70 kHz	D_4	1.5KE16

Simultaneously, L_C starts taking current at constant voltage from the boost inductor

$$i_{L_C}(t) = i_{L_C}(t_4) + \frac{1}{L_C}\int_{t_4}^{t}\left[v_I - \frac{(v_I - V_O)\,N_1}{N_1 + N_2}\right]d\tau = \frac{1}{L_C}\left[v_I - (v_I - V_O)\,\frac{N_1}{N_1 + N_2}\right](t - t_4). \quad (59)$$

This state ends when L_C takes the output current, the whole magnetizing current of the tapped boost inductor, and D_A turns off

$$i_{L_C}(t_5) = i_{L_M} = \frac{1}{L_C}\left[v_I - \frac{(v_I - V_O)\,N_1}{N_1 + N_2}\right](t_5 - t_4). \quad (60)$$

- $t_5 < t \leq t_6$ (Figure2i): The state evolves with current i_{L_S} oscillating according to Equation (58) until diode D_E turns off. We solve

$$0 = \frac{V_O}{2}\sqrt{\frac{C_S}{L_S}}\sin\left(\frac{t_6 - t_4}{\sqrt{L_S C_S}}\right), \quad (61)$$

in order to find

$$t_6 - t_4 = \pi\sqrt{L_S C_S}. \quad (62)$$

Thus, capacitor C_S ends charged with

$$v_{C_S}(t_6) = \frac{V_O}{2}, \quad (63)$$

which is the voltage needed in the next mode II turn-on switching to produce ZVS.

- $t_6 < t \leq T_S + t_0$ (Figure2a) ON-State.

The waveforms for this mode are similar to those pictured in Figure 3. The differences lie in the characteristic values and in the $i_{L_S}(t)$ plot, which presents a complete resonant half cycle up to t_6 instead of the linear discharge.

3. EXPERIMENTAL RESULTS

Figure 4 shows the complete schematic of the boost PFC module. In order to control the power factor corrector, we used the UC3854 integrated circuit [24, 23], which implements average input current control [1]. The controller provides both output voltage regulation and sinusoidal input current.

The input current is indirectly measured with current transformers CT_1 and CT_2 as proposed in [24]. Extra diodes D_3 and transient voltage suppressor D_4 were included to clamp overvoltages produced by CT_2 leakage inductance.

The voltage source V_X is implemented as proposed in Figure 10b with a 47 μF capacitor, a 1 kΩ resistor and diode D_5, in order to return some of the energy to the input and improve the efficiency. The value of the clamp resistor was experimentally adjusted to set the desired value of $V_X = V_O/2$, as we derived in Section 2..

Table 1 lists the complete specifications and significant components of the prototype. Figure 5 is a photograph of the prototype and shows the relative sizing of the main inductive components.

3.1. Switching Waveforms

We have captured switch voltage and current waveforms for output powers of 1.5 kW (Figure6) and 3 kW (Figure7). Both were measured near the peak input voltage. Some features that we described in the theoretical waveforms of Figure 3 are present: the slowly rising current during turn-on, the resonant oscillation of capacitor C_S with inductor L_S, and the linearly increasing voltage during turn-off.

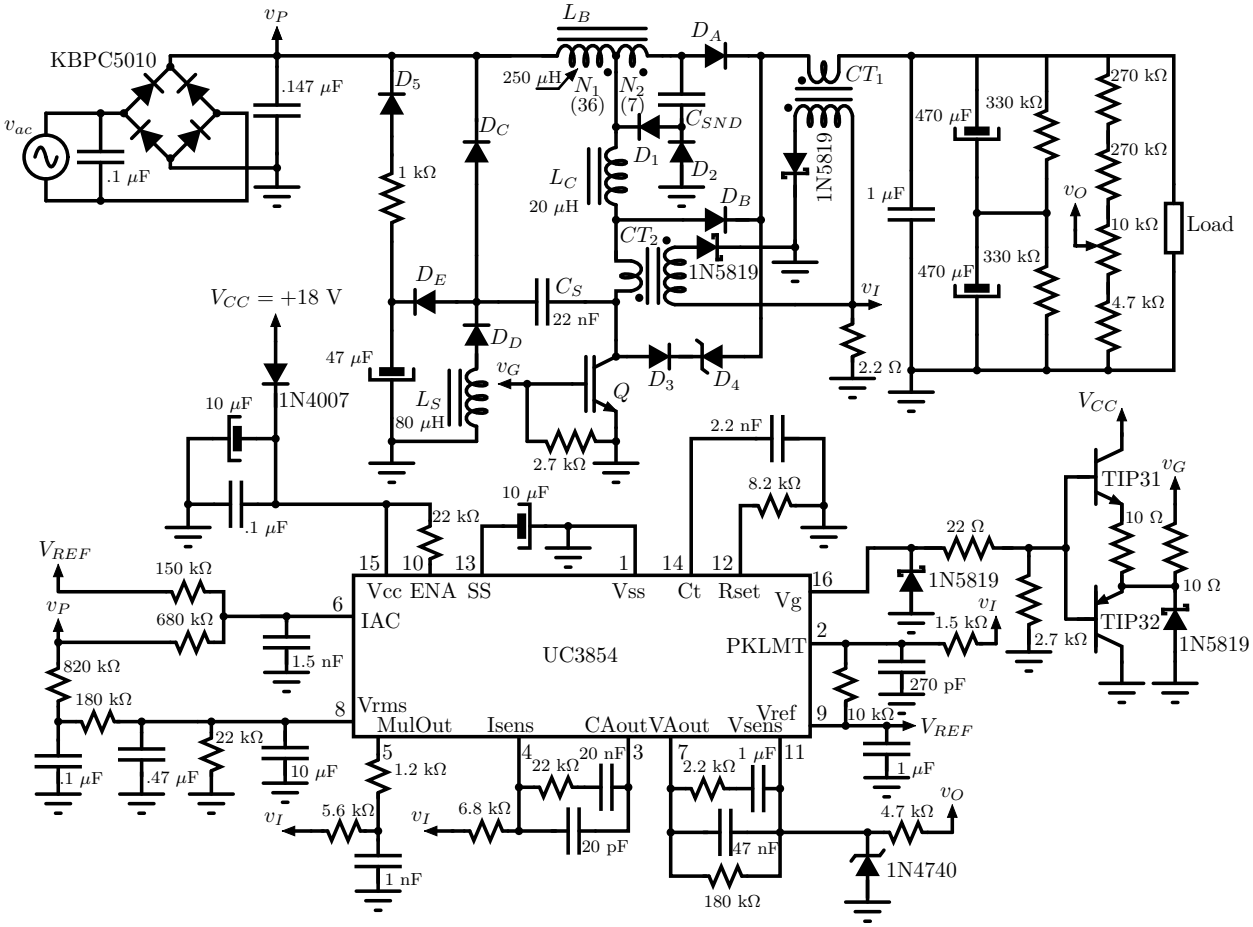

Figure 4. Complete circuit schematic of the boost PFC module.

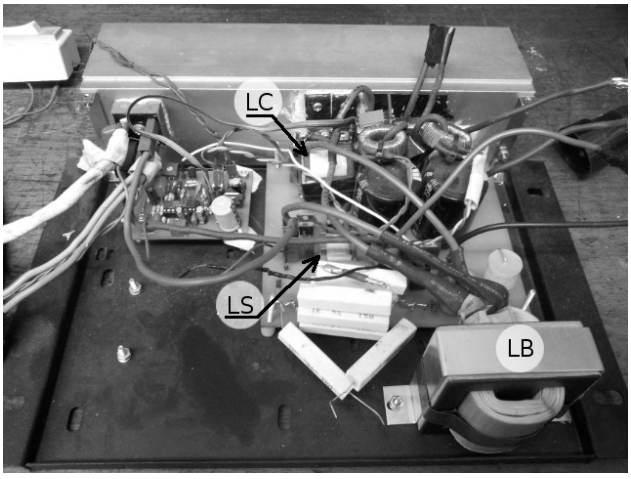

Figure 5. Photograph of the 3 kW prototype. The main inductive components are labeled.

Additional non-ideal features appear: IGBT tail current and transistor turn-off overvoltage in Figure 6c — limited by the non-dissipative snubber of Figure 1a—, inductor current ripple and overdamped oscillation of switch voltage after L_C discharges (Figure6a).

Unmodeled parasitic components produce some of the features present in Figure 7a, which are not justified in the theoretical waveforms of Figure 3 or observable in Figure 6a. For example, we added diodes D_3 and D_4 in order to reach the final nominal power of 3 kW. These diodes were removed to measure the waveforms of Figure 6a.

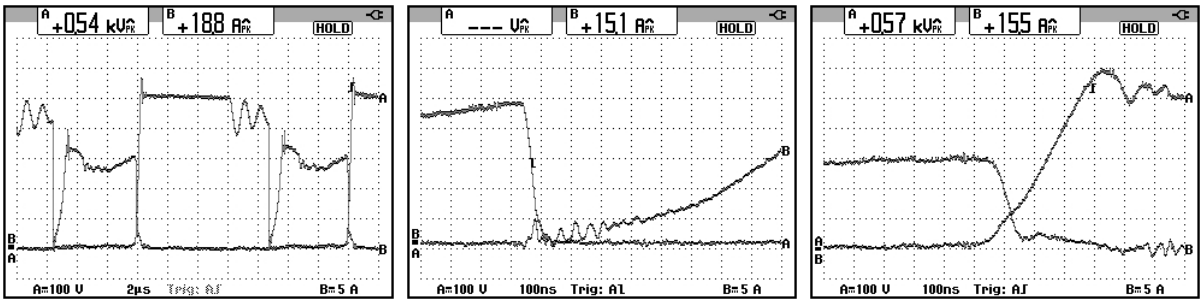

(a) Full switching cycle. (b) Turn-on detail. (c) Turn-off detail.

Figure 6. Switch voltage v_{CE} (A) and current i_C (B). $P_O \simeq 1.5$ kW. Diodes D_3 and D_4 disconnected.

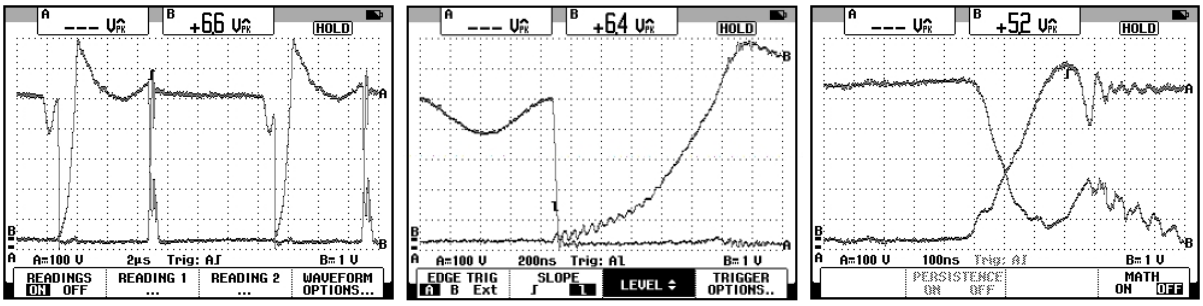

(a) Full switching cycle. (b) Turn-on detail. (c) Turn-off detail.

Figure 7. Switch voltage v_{CE} (A) and current i_C (B). $P_O \simeq 3$ kW.

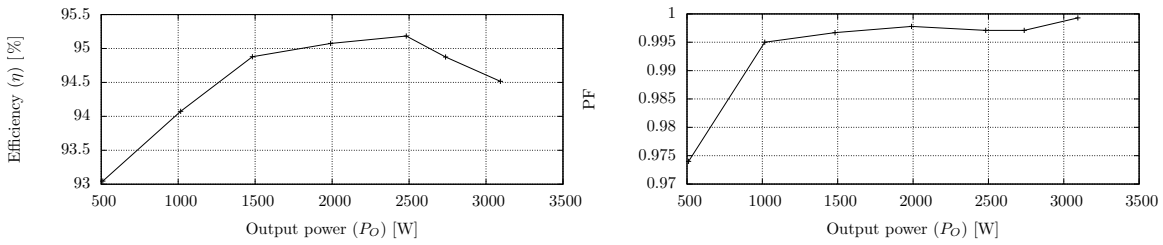

(a) Efficiency . (b) Power factor.

Figure 8. Efficiency and power factor of the converter presented in Figure4 for varying output power.

Figure 6a presents the switch voltage superimposed with the switch current to show the switching transitions. Figure 6b presents the detailed ZCS turn-on transition and Figure 6c the near ZVS turn-off. Despite the presence of non-zero voltage during the turn-off transition, a piecewise-linear approximation to the waveforms allowed us to estimate a reduction of 93.3% in turn-off losses, compared to the hard switching case. Figure 7 displays the same waveforms and detailed transitions as in the previous case. The near ZVS turn-off is more evident for this output power level (Fig. 7c).

3.2. Power factor and efficiency

Figure 8 presents the efficiency and power factor measurements made for various load conditions. The power factor is higher than 0.975 (Figure8b) and the prototype attains efficiencies higher than 93% (Figure8a).

The input voltage and current waveforms are presented in Figure 9. Despite the presence of zero crossing distortion, the power factor is at a peak value as depicted by Figure 8b.

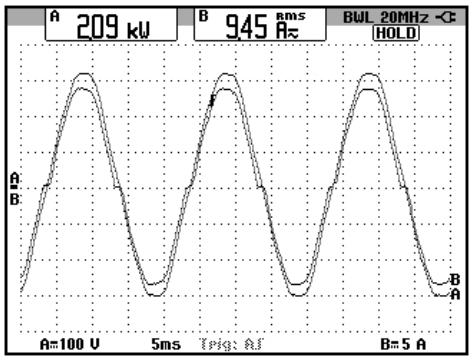

Figure 9. Input voltage (A) and current (B) waveforms for $P_O \simeq 2$ kW.

4. MODULAR SYSTEM CONFIGURATIONS

In order to employ the converter in modular designs, the energy extracted by the soft-switching cell has to be redirected or dissipated; Figure 10 shows different options to manage the power extracted. The simplest method is to dissipate the energy with a resistor, as shown in Figure 10a. This solution is inexpensive but compromises the efficiency, which is not advisable for high power applications: the amount of dissipated heat requires forced air cooling, reducing the reliability of the system. The second method is a variation of the first in which part of the energy returns to the source and part is dissipated in the resistor (see Figure10b).

The third alternative in Figure 10c exploits part of the energy to power the auxiliary circuitry. It needs a careful design in order to provide enough energy for all loads and it could be complementary of the previous two methods.

The last option, in Figure 10d, is the most efficient method but also the most expensive. The idea is to transfer the energy to the output using a boost converter. It is also the ideal solution for high power modular applications, where a boost soft-switched module may provide regulation of the clamping voltage V_X with high efficiency conversion. However, the control of this module should be modified in order to regulate the input voltage to $V_X = V_O/2$ instead of the output voltage.

The first three alternatives should be applied in a per module approach: each module must provide its resistor, to even the distribution of heat among modules, and/or to power its auxiliary circuits, so as to avoid compromising the reliability and to take advantage of redundancy. The last one is more adequate for fully modular systems: all the V_X outputs connect to the input of the auxiliary converter, which can be a classical boost converter or one of the soft-switched module; this is interesting in the case of higher power applications, such as in locomotive power supplies or electric car fast battery chargers.

5. CONCLUSION

We studied, constructed and tested a modified boost PFC with additional soft-switching passive networks using a commercial integrated controller. The proposed converter exhibits lower switching losses than a classical boost and power factor correction. The 3 kW prototype can integrate higher power multimodular single phase and three-phase power supplies. The experimental evidence shows that the module has an efficiency greater than $93\,\%$ with near unity power factor for several load conditions. Using ancillary recovery converter modules higher efficiencies could be expected.

We have shown the need of a voltage source to produce ZVS turn-off for the whole input voltage cycle and we have introduced a variety of schemes in order to provide it. The experimental converter dissipates the power transferred to the voltage source in a resistor; the efficiency could increase if, instead of the resistor, an additional converter transferred the energy to the output. This alternative becomes very attractive in higher power multimodular applications, where one of the modules can fulfill this task.

ACKNOWLEDGMENT

The authors wish to acknowledge the different funding sources that allowed the completion of this work. The 2014/17 UBACYT grant (20020130100840BA) equipped us with some of the instruments and provided materials used in this work. A Fundacin YPF grant was used to obtain the digital wattmeter. A technology transfer agreement signed between HT S.A. and the University of Buenos Aires granted materials, components, and student internship

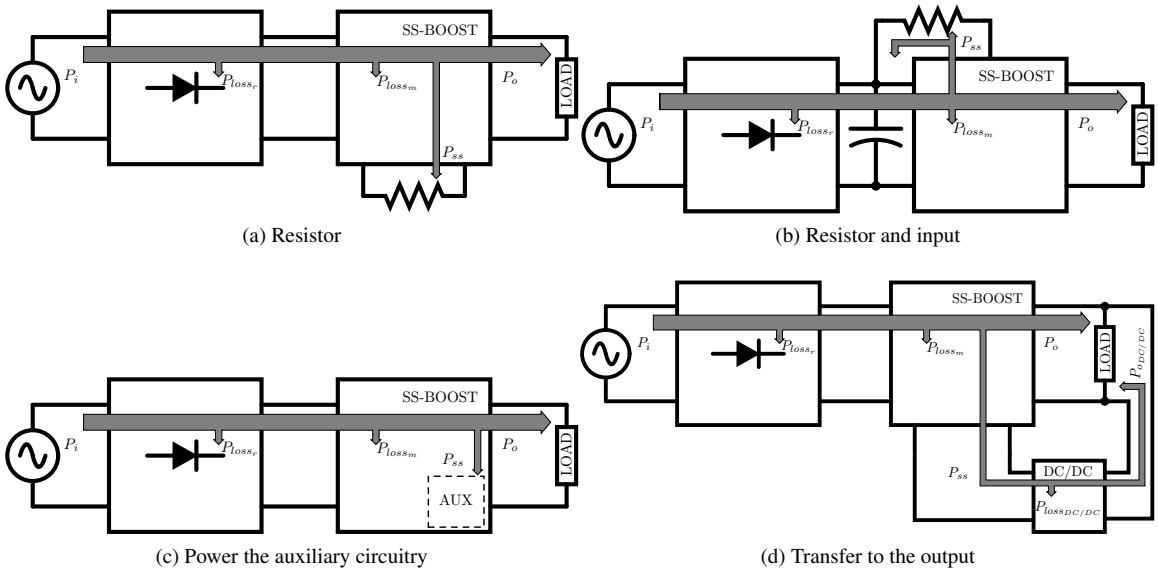

(a) Resistor (b) Resistor and input

(c) Power the auxiliary circuitry (d) Transfer to the output

Figure 10. Different methods to manage the power extracted by the soft-switching cell.

salaries. The work of T. A. G. was sponsored by a scholarship from CONICET.

REFERENCES

[1] R. W. Erickson and M. Dragan, *Fundamentals of Power Electronics*, 2nd ed. Springer, 2001.

[2] D. Lenine, Ch. Sai Babu, G. Shankaraiah, "Performance Evaluation of Fuzzy and PI Controller for Boost Converter with Active PFC," *International Journal of Power Electronics and Drive Systems*, vol. 2, no. 4, pp. 445–453, Dec. 2012. [Online]. Available: http://iaesjournal.com/online/index.php/IJPEDS/article/view/522/935

[3] Ajeesh G. and Jayakumar M. S., "A High Efficient High Input Power Factor Interleaved Boost Converter," *International Journal of Electrical and Computer Engineering*, vol. 2, no. 3, pp. 339–344, Jun. 2012. [Online]. Available: http://iaesjournal.com/online/index.php/IJECE/article/view/254

[4] M. R. Kumar, D. Lenine, and C. S. Babu, "A Variable Switching Frequency with Boost Power Factor Correction Converter," *TELKOMNIKA (Telecommunication Computing Electronics and Control)*, vol. 9, no. 1, p. 47, Apr. 2011. [Online]. Available: http://journal.uad.ac.id/index.php/TELKOMNIKA/article/view/644

[5] Z. Lu and T. Green, "A study of soft-switched CCM boost AC/DC converter," in *Seventh International Conference on Power Electronics and Variable Speed Drives, 1998. (Conf. Publ. No. 456)*, 1998, pp. 662–667. [Online]. Available: http://ieeexplore.ieee.org/xpls/abs_all.jsp?arnumber=732138

[6] G. Moschopoulos and S. Li, "A soft-switched AC-DC boost converter with power factor correction and reduced switch voltage stress," in *Canadian Conference on Electrical and Computer Engineering*, vol. 1, 2003, pp. 375–378 vol.1. [Online]. Available: http://ieeexplore.ieee.org/xpls/abs_all.jsp?arnumber=1226419

[7] L. Barreto, "Analysis of a soft-switched PFC boost converter using analog and digital control circuits," *IEEE Transactions on Industrial Electronics*, vol. 52, no. 1, pp. 221–227, Feb. 2005. [Online]. Available: http://ieeexplore.ieee.org/xpls/abs_all.jsp?arnumber=1391111

[8] Y. Jang and M. Jovanovic, "High-power-factor soft-switched boost converter," *IEEE Transactions on Power Electronics*, vol. 21, no. 1, pp. 98–104, Jan. 2006. [Online]. Available: http://ieeexplore.ieee.org/xpls/abs_all.jsp?arnumber=1566694

[9] H. Suryawanshi, M. Ramteke, K. Thakre, and V. Borghate, "Unity-Power-Factor Operation of Three-Phase ACDC Soft Switched Converter Based On Boost Active Clamp Topology in Modular Approach," *Power Electronics, IEEE Transactions on*, vol. 23, no. 1, pp. 229–236, Jan. 2008.

[10] S. Saha, B. Majumdar, and S. Biswas, "Improved active power factor correction circuit using a fully soft-switched boost converter," *IET Power Electronics*, vol. 4, no. 7, p. 835, 2011. [Online]. Available: http://digital-library.theiet.org/content/journals/10.1049/iet-pel.2010.0079

[11] B. Akn and H. Bodur, "A New Single-Phase Soft-Switching Power Factor Correction Converter," *IEEE Transactions on Power Electronics*, vol. 26, no. 2, pp. 436–443, Feb. 2011. [Online]. Available:

http://ieeexplore.ieee.org/lpdocs/epic03/wrapper.htm?arnumber=5524036
[12] M. Mahesh and A. Panda, "High-power factor three-phase ac-dc soft-switched converter incorporating zero-voltage transition topology in modular systems for high-power industry applications," *Power Electronics, IET*, vol. 4, no. 9, pp. 1032–1042, Nov. 2011.
[13] M. Mahesh and A. K. Panda, "A high performance single-phase AC-DC PFC boost converter with passive snubber circuit," in *2012 IEEE Energy Conversion Congress and Exposition (ECCE)*. IEEE, Sep. 2012, pp. 2888–2894. [Online]. Available: http://ieeexplore.ieee.org/lpdocs/epic03/wrapper.htm?arnumber=6342370
[14] H.-S. Kim, J.-W. Baek, J.-H. Jung, J.-H. Kim, M.-H. Ryu, and H.-J. Kim, "A boost PFC rectifier with a passive lossless snubber circuit using coupled inductors methods," in *2012 Twenty-Seventh Annual IEEE Applied Power Electronics Conference and Exposition (APEC)*. IEEE, Feb. 2012, pp. 1148–1152. [Online]. Available: http://ieeexplore.ieee.org/lpdocs/epic03/wrapper.htm?arnumber=6165963
[15] R. Li, H.-H. Chung, and A. Sung, "Passive Lossless Snubber for Boost PFC With Minimum Voltage and Current Stress," *IEEE Transactions on Power Electronics*, vol. 25, no. 3, pp. 602–613, Mar. 2010. [Online]. Available: http://ieeexplore.ieee.org/lpdocs/epic03/wrapper.htm?arnumber=5299121
[16] V. Ramesh, Y. Kusuma Latha, "A Soft Switching Control Strategy Based on Interleaved Boost Converter for BLDC Motor Drive," *International Journal of Power Electronics and Drive Systems*, vol. 6, no. 3, pp. 516–523, Sep. 2015. [Online]. Available: http://iaesjournal.com/online/index.php/IJPEDS/article/view/7880/pdf7880
[17] J. Noon, "UC3855A/B High Performance Power Factor Preregulator," p. 35, 2004. [Online]. Available: http://www.ti.com/lit/an/slua146a/slua146a.pdf
[18] S. Luo, "A review of distributed power systems part I: DC distributed power system," *IEEE Aerospace and Electronic Systems Magazine*, vol. 20, no. 8, pp. 5–16, Aug. 2005. [Online]. Available: http://ieeexplore.ieee.org/lpdocs/epic03/wrapper.htm?arnumber=1499272
[19] C. Moo, H. Cheng, and P. Lin, "Parallel operation of modular power factor correction circuits," *Power Electronics, IEEE Transactions on*, vol. 17, no. 3, pp. 398–404, May 2002.
[20] D. Jia and L. Yang, "Parallel high-power inverting power supply for DJ1 locomotive," in *2009 9th International Conference on Electronic Measurement & Instruments*. IEEE, Aug. 2009, pp. 4–659–4–663. [Online]. Available: http://ieeexplore.ieee.org/lpdocs/epic03/wrapper.htm?arnumber=5274673
[21] M. Yilmaz and P. T. Krein, "Review of Battery Charger Topologies, Charging Power Levels, and Infrastructure for Plug-In Electric and Hybrid Vehicles," *IEEE Transactions on Power Electronics*, vol. 28, no. 5, pp. 2151–2169, May 2013. [Online]. Available: http://ieeexplore.ieee.org/lpdocs/epic03/wrapper.htm?arnumber=6280677
[22] G. Spiazzi and F. Lee, "Implementation of single-phase boost power-factor-correction circuits in three-phase applications," *IEEE Transactions on Industrial Electronics*, vol. 44, no. 3, pp. 365–371, Jun. 1997. [Online]. Available: http://ieeexplore.ieee.org/lpdocs/epic03/wrapper.htm?arnumber=585834
[23] Texas Instruments, "UC1854, UC2854, UC3854 High Power Factor Preregulator," p. 12, 1998. [Online]. Available: http://www.ti.com/product/uc3854
[24] P. C. Todd, "UC3854 controlled power factor correction circuit design," p. 21, 1999. [Online]. Available: http://www.ti.com/lit/an/slua144/slua144.pdf

BIOGRAPHIES OF AUTHORS

Toms A. Gonzlez was born in Buenos Aires, Argentina, in 1983. He received the B.E. degree in electrical engineering from the University of Buenos Aires in 2010 and he is currently working towards his Ph.D.. Since 2007, he has been instructor at the Department of Electrical Engineering in the areas of Basic Electronics and Control Theory. His main research interests are power factor correction, SMPS, and LED lighting.

Daniel O. Mercuri was born in Buenos Aires, Argentina in 1980. He received the B.E. degree in electrical engineering from the University of Buenos Aires in 2015. His research and development interests are soft-switched conversion, high voltage power supplies and high efficiency power converters. He currently works with the National Comission of Atomic Energy (CNEA) to develop high-voltage switching power supplies.

Hernn E. Tacca was born in Argentina on December 15, 1954. He received the B.E. degree in electrical engineering from the University of Buenos Aires (Argentina), in 1981 and the M.S. and Ph.D. degrees from the University of Sciences and Technologies of Lille (France) in 1988 and 1993 , respectively. In 1998 he received the Doctorate degree from the University of Buenos Aires. Since 1984 , he has been with the Faculty of Engineering of the University of Buenos Aires, where he is currently Assistant Professor and engaged in teaching and research in the areas of industrial electronics. His research interest are in the field of SMPS, UPS, battery chargers, soft-switching techniques and microcontroller control of power converters.

Mximo E. Pupareli was born in Argentina on April 15, 1941. He received the B.E. in electrical engineering from the University of Tucumn (Argentina) in 1867. He has worked as Professor in the area of Electronic Materials Technology and as developer in the Institute of Space Physics and Astronomy (CONICET). From 1975 to 1985 he was Vice Director at the Institute of Space Physics and Astronomy. Since 1985, he has been involved exclusively in the business activities in the field of development and manufacturing of electronic devices at H.T. S.A..